Hydromechanical Model of Geological Carbon Sequestration in Saline Aquifers

J. A. Torres[1*], I. Bogdanov[1] and M. Boisson[2]
1. Computational Hydrocarbon Laboratory for Optimized Energy Efficiency (CHLOE), University of Pau, Pau, 64013, France.
2. Total SA, Centre Scientifique et Technique Jean Féger (CSTJF), 64000 Pau, France.

*Corresponding author: jose-antonio.torres@univ-pau.fr

Abstract

The ability to perform reliable reservoir simulations is paramount for the success of Geological Carbon Storage (GCS) projects. Reservoir modeling and simulation exercises are required along the whole GCS project lifecycle: to inform or guide site screening assessments, execute feasibility studies, design monitoring techniques, support operations, and to evaluate potential risks. However, these models are data-intensive, and many times not all the required data is available, especially at the early stages of a project. More specifically, it is not unusual that the faulted zones are poorly characterized, despite the fact that this is an important factor both for fluid flow and geomechanical modelling. In this context, our work deals with a conceptual model intended to test modelling features aimed at studying potential risks of fluid migration out of the reservoir zone, even without having detailed characterization of the faulted zone. A synthetic 2D model was built and used to show how certain modeling features can help to gain understanding about fault activation mechanisms, which govern the complex interaction between mechanical deformation and fluid flow evolution in a deep reservoir. The model particularly illustrates when and how local overpressure perturbs the faulted region state, causes sufficient mechanical deformation and triggers enhancements of the fault permeability, creating new high-permeability pathways for possible CO_2 leakage flow. Results indicate that the dynamics of the fault permeability is a critical factor, one of those which are possible to evaluate for CO_2 injection scenarios in complex geological formations using this type of models.

1. Introduction

Injectivity, capacity, and containment integrity are three key elements for any Geological Carbon Storage (GCS) project. These factors could be greatly influenced by hydro-mechanical processes during and after CO_2 injection. For instance, if the injection is not properly managed, average pressure in the reservoir could increase and change the state of effective stresses. Sometimes the overpressure could affect the mechanical integrity of the caprock, increasing the potential risks of the process. Therefore, reservoir management strategy is necessary for reducing risks associated with the fluid injection.

Coupled fluid and geomechanics simulation is one of reservoir management tools for analyzing various issues associated with fluid injection (Rutqvist et al, 2012). Previously published works have demonstrated how simulations can be used to explain or predict complex hydro-mechanical mechanisms. For instance, Bjornara et al (2010) have shown that the uplift observed during the In Salah demonstration project could be explained using a poroelastic model containing faulted zone and high-permeability pathways. Their model based on the Biot's poroelasticity theory, accounts for elastic mechanical responses to injection of fluid into a low permeability formation. Eventually, the injection caused the expansion of the upper geological formations. More recently, Nguyen et al (2019) developed a numerical model to investigate fault behavior during the experiment of controlled water injection in a fault at the Mont-Terri Underground Research Laboratory in Switzerland. Their model based on the classical theory of poromechanics and Coulomb's friction, correctly predicted that the overpressure caused by the fluid injection produces a decrease in the effective stress leading to fault activation and a significant increase of permeability in the faulted region.

It is well-known that reliable hydro-mechanical models need suitable site-specific characterization. Unfortunately, many times not all the desirable data is available. This situation is more common during the first stages of a project. In particular, for a number of reasons faulted zones characterization carries out many uncertainties. In this context, our work presents a conceptual model to quickly investigate potential risks of fluid migration out of the reservoir zone after fault re-activation. The model uses empirical correlations, which could help in project stages when there is not available a detailed characterization of the faulted zone.

We built our 2D model following a known case study by Cappa and Rutqvist (2011) which addresses complex fault behaviors in the typical framework of fluid injection. We tested several modeling features that help to gain understanding about complex fault mechanisms. Empirical correlations found in literature were used for modeling changes in porosity and permeability with the volumetric strain. The model uses COMSOL Multiphysics' Poroelasticity interface that couples Darcy's law and Solid Mechanics equations to evaluate deformation of the porous media as a consequence of fluid injection (COMSOL 2018). A fully-coupled procedure is followed to solve the hydro-mechanical model. At this stage the model assumes single-phase fluid flow, linear elasticity, and the stress regime below the Coulomb criterion. Soil plasticity is considered as a separated feature, just to analyze the extent of the failure zone at selected time-steps.

2. Governing Equations

The model relies on the Poroelasticity Multiphysics interface, which links Darcy's law and Solid Mechanics interfaces (COMSOL 2018). For the sake of completeness and transparency, we reproduce below the key equations implemented in the COMSOL Multiphysics Poroelasticity interface.

The poro-elasticity theory provides the relation between the stress change $\boldsymbol{\sigma}$ in an elastic porous media to the linearized strain $\boldsymbol{\varepsilon}$ and the change in fluid pressure *p*

$$\boldsymbol{\sigma} = \boldsymbol{C}\colon \boldsymbol{\varepsilon} \; - \alpha p \boldsymbol{I} \tag{1}$$

where $\boldsymbol{C}$ and α are the (fourth-order) elasticity tensor and Biot coefficient. The symbol *":"* represents a double-dot tensor product (or contraction over two indices). It is assumed that the evolution of the geological structures occurs under quasi-static conditions and the equations for mechanical equilibrium are enforced

$$\nabla \cdot \boldsymbol{\sigma} + \boldsymbol{F_V} = \mathbf{0} \tag{2}$$

where $\boldsymbol{F_V}$ represents the body forces acting over the geometry, and the term ∇ represents a divergence operator.

On the other hand, according to the Darcy's law (see equation (3)), the net flux across a representative elementary volume of a porous media is linearly proportional to the flow capacity (permeability over fluid viscosity), and linearly proportional to the driven force, the velocity potential (Bear, 1988).

$$\boldsymbol{u} = -\frac{\boldsymbol{k}}{\mu}(\nabla p + \rho \boldsymbol{g} \nabla \cdot \mathbf{D}) \tag{3}$$

where $\boldsymbol{u}$ represents the Darcy's velocity including fluid and solid matrix properties, the permeability tensor $\boldsymbol{k}$, fluid viscosity, μ, fluid density, ρ, and acceleration of gravity, $\boldsymbol{g}$.

The equation of mass conservation or continuity equation for a representative elementary volume takes the form,

$$\frac{\partial(\rho \varepsilon_p)}{\partial t} + \nabla \cdot (\rho \boldsymbol{u}) = Q_m \tag{4}$$

where ε_p is the porosity, $\frac{\partial(\rho \varepsilon_p)}{\partial t}$ represents the accumulation term per unit volume, $\nabla \cdot (\rho \boldsymbol{u})$ represents the net flux in a control volume, and the expression Q_m represents a source term (or increment in fluid content due to the pore volume change), proportional to the rate of the pore volume deformation,

$$Q_m = \rho \alpha \frac{\partial \varepsilon_{vol}}{\partial t} \tag{5}$$

Here, ε_{vol} represents the volumetric strain of the matrix. By applying the chain rule, the first term on equation (5) can be expanded in a way that we get the linearized storage coefficient *S*,

$$\frac{\partial(\rho \varepsilon_p)}{\partial t} = \rho\left(\varepsilon_p c_f + \varepsilon_p c_p\right)\frac{\partial p}{\partial t} = \rho S \frac{\partial p}{\partial t} \tag{6}$$

where c_f is the fluid compressibility $\frac{1}{\rho}\frac{\partial \rho}{\partial p}$, and the term $c_p$is the rock compressibility expressed as $\frac{1}{\varepsilon_p}$ $\frac{\partial \varepsilon_p}{\partial p}$.

The term *S* can be interpreted as the weighted compressibility of the solid and fluid present in a given pore volume. Usually, S can be expressed as a function of the drained bulk modulus, K_d, and the fluid bulk modulus, K_f;

$$S = \frac{\varepsilon_p}{K_f} + (\alpha - \varepsilon_p)\frac{(1-\alpha)}{K_d} \tag{7}$$

The governing equation for the Darcy's Law interface results from combining the above equations as follows,

$$\rho S \frac{\partial p}{\partial t} - \nabla \cdot \left(\rho\left[\frac{\boldsymbol{k}}{\mu}(\nabla p + \rho \boldsymbol{g} \nabla \cdot \mathbf{D})\right]\right) = Q_m \tag{8}$$

Note that equation (8) reflects the coupling between fluid flow pressure and mechanical deformation of the material, implicit in the term Q_m.

The following empirical correlations were used for modeling changes of porosity and permeability with the mechanical deformation of the rock, (Mainguy and Longuemare, 2002; Ihsan 2018):

$$k = k_i * \left(\varepsilon_p/\varepsilon_{p,i}\right)^n \quad \textbf{(9)}$$

$$\varepsilon_p = \varepsilon_{p,i} * (1 - \varepsilon_{vol}) \quad \textbf{(10)}$$

where ε_{vol} refers to the volumetric strain, and the sub-index *i* refers to the initial state.

For the faulted zone we used a simple modeling approach to represent the effect of the permeability variation as a consequence of the pressure perturbation. Our approach was inspired by field experimental observations presented in Guglielmi et al (2017), and the theoretical work proposed by Ghanimi et al (2017). On one hand, Guglielmi et al (2017) observed that the fault transmissibility at the Mont Terri Main Fault increased from 5 to 6 orders of magnitude for a very small amount of cumulated strain. On the other hand, Ghanimi et al (2017) proposed a simple theoretical approach to model stress-sensitivity permeability before the stress regime becomes critical. In our work, the change in permeability in the faulted zone was a step function of the cumulative strain,

$$k_f = \begin{cases} k_{f,min} & if(\varepsilon_{vol} < \varepsilon_\delta) \\ k_{f,max} & if(\varepsilon_{vol} > \varepsilon_\delta) \end{cases} \quad \textbf{(11)}$$

where ε_δ is a model parameter, defined as the threshold volumetric deformation that triggers the fault permeability enhancement. Our assumption that the stress regime is below the Coulomb criterion can be seen as a conservative assumption, in the sense that small deformations of the faulted region might represent a risk of leakage, even though the fault may still have not experience a major slip event.

3. Model description

While in general the 2D model followed the model proposed by Cappa and Rutqvist (2011), some modifications were made to the original base case. For example, the Solid Mechanics equations follow the Plain Strain and quasi-static assumptions. Also the Darcy's Law equation was used to simulate time-dependent single-phase flow, which particularly corresponds to the conditions when the CO_2 is dissolved into injected aqueous solution. The pressure dependency of fluid properties (density, viscosity, and compressibility) is neglected.

Regarding the mechanical constitutive equations, the model considers mostly linear elasticity, except for the faulted zone, where we added the Soil Plasticity material model and the Mohr-Coulomb failure criterion to simulate elastoplastic behavior (both features, part of the Geomechanics module, where implemented into a second Study step). These features applied in post-processing steps allowed us to analyze, for selected times, the degree of instantaneous material failure and its possible consequences.

Initial state of stresses (before injection), was defined using the "Initial Stress and Strain" feature (Solid Mechanics module). Three types of mechanical boundary conditions were defined: 1) constant pressure load at the top boundary, 2) roller conditions at the right-side and bottom boundaries, and 3) horizontal stress at the left-side boundary. A rigid body was incorporated at the left boundary, as a way to apply a uniform load among all the different layers.

No-flow boundary conditions were used at all boundaries except for the lateral aquifer boundaries that had open boundary conditions with hydrostatic pressure gradient as constraint. The well is controlled with a constant injection rate condition at the wellbore perforation (at the following position: x=0, y=-1500m).

Figure 1a illustrates the model geometry, the FEM mesh is shown in Figure 1b, and the initial stress and hydrostatic pressure gradients in Figure 1c. The mesh consists of 10062 elements, having a total of 59871 degrees of freedom, with minimum quality of 0.5772 and average quality of 0.8911. Model parameters such as domain geometry dimensions, material properties, fluid properties, and well parameters are listed in the Table 1.

The faulted-zone is modeled using a volumetric region with a width of 10m (damaged zone around a main fault) and equivalent initial permeability of 10^{-16} m².

Notice that, by accounting for the evolution of the fault permeability as a function of the volumetric strain, we did introduce a strong nonlinearity in the model under consideration. For that reason, we used three different techniques for improving the convergence of the model: 1) definition of a step-load for the mass flow rate, 2) activation of the "Auxiliary sweeps" feature with the fluid compressibility as sweep parameter, and 3) settings adjustments in the "Fully Coupled" solver feature, including maximum number of iterations and nonlinear solution method.

Mention that for many reasons, the physical principles discussed above are particularly appealing for modeling the fault behavior. For

example, the method can be extrapolated to 3D geometries. Additionally, the evaluation of multiple scenarios like initially closed, opened or semi-opened fault to fluid flow may be envisaged. Also, the coupled model is compatible with dynamic probabilistic risk assessment, as it provides physical parameters which may be put into practice using uncertainty quantification methods. Next section will present a couple of calculation examples using a synthetic case study adapted after the model proposed by Cappa and Rutqvist (2011).

4- Results and discussion

Two study cases were considered:

- Case 1: solving the fully-coupled flow and geomechanical model, without permeability enhancements in the faulted zone (i.e. with equation (11) disabled),
- Case 2: solving the fully-coupled flow and geomechanical model, incorporating the evolution of permeability in the faulted zone (equation (11) enabled).

Using the fully-coupled approach, the system of equations is solved simultaneously, taking a CPU time of approximately 5 minutes with 59871 of degrees of freedom (DOFs) solved for (plus 10380 internal DOFs). We ran the cases using a Dell Precision 3630 Tower with the following hardware specifications: Intel Xeon E Processor E-2146G, 6 Core and 3.5 GHz; and 48 Gb RAM.

Figure 2 shows the evolution of the average pressure in each layer for the study cases; Case 1 is represented with continuous lines, while Case 2 with dashed lines. The pressure increased significantly in the Storage Reservoir (Fig 2b). The most severe overpressure inside the Storage Reservoir occurred for the Case 1. Moderate average pressure increases were also observed for the Upper and Basal Aquifers (Fig 2a) and for the Upper and Lower Caprocks (Fig 2b).

Figure 3 shows the pressure maps after 10 years of injection jointly with the permeability maps. Permeability enhancement in the faulted zone was caused by the local volumetric strain changes, according to equation (11).

On one hand, Case 1 pressure map (Fig 3a) reveals a significant pressure increase in the Storage Reservoir, with a maximum pressure value of 37.7 MPa. Furthermore, Case 1 permeability map (Fig 3b) shows that the fault permeability is 3 orders of magnitude lower than the reservoir permeability. This difference in permeability caused that the fault operated as a flow barrier. Pressure increased significantly inside the storage reservoir (see the left compartment, between the injection point and the faulted zone in Fig 3a), with the faulted region serving as a mechanical containment.

On the other hand, Case 2 results show a different scenario. Figure 3c shows that the pressure extensively diffuses into the aquifers, with the maximum pressure being equal to 26.2 MPa. The pressure contours indicate better communication across the fault. The main factor explaining differences between Case 1 and Case 2 is the permeability enhancement in the fault, which was of six orders of magnitude (from 10^{-16} m^2 up to 10^{-10} m^2 [cf. Figures 3b and 3d]). Changes in permeability are driven by the volumetric deformation in the faulted zone which intersects the storage reservoir and the aquifers (Fig 1). These permeability changes opened high-permeability pathways which facilitated the fluid flow, releasing somewhat the overpressure generated by the injection.

To summarize, without enhancement of the faulted-region permeability, the model predicts a scenario of fluid containment. Under this scenario, there is an important overpressure inside the storage reservoir, where the fault acts as a flow barrier. With the faulted-region permeability enhancement feature enabled, the model predicts changes in the fault permeability, which in turn affects the fluid flow pathways. Consequently, the pressure diffuses into those geological units that are in better communication during and after the injection.

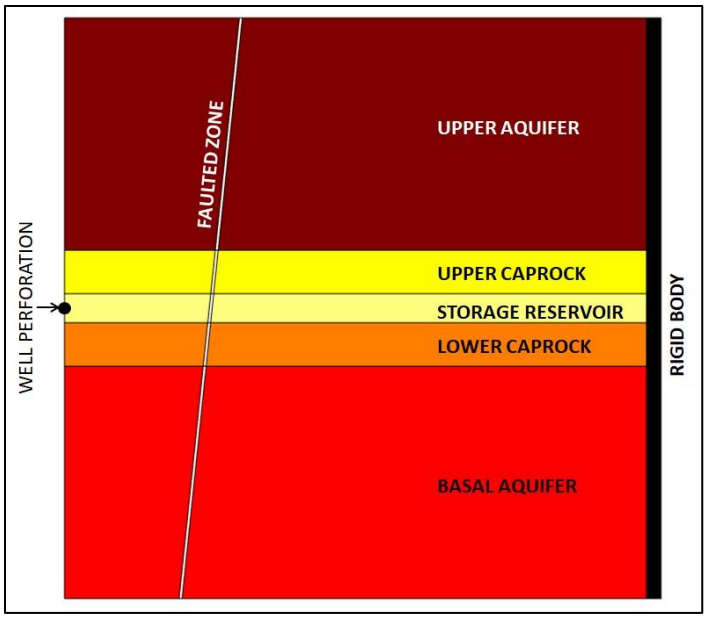

(a) Model geometry

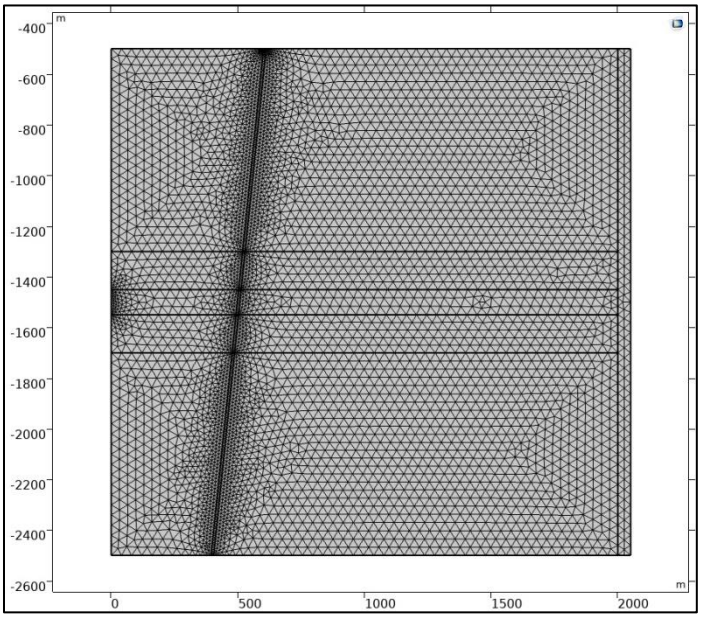

(b) FEM mesh

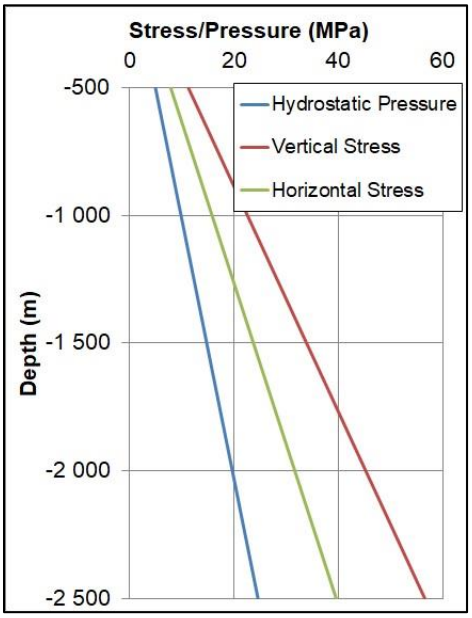

(c) Stress gradients and the hydrostatic pressure gradient

Figure 1. Illustrations of the model geometry (a), the FEM mesh (b), and the stress/pressure vertical gradients (c). In the top-left corner the model geometry is shown: from top to bottom, there are five different rock layers that are classified as follows: Upper Aquifer, Upper Caprock, Storage Reservoir, Lower Caprock, and Basal Aquifer. In the bottom-left corner the FEM mesh is illustrated that was created using triangular elements; the mesh density is higher near the (well) perforation point and around the faulted region. On the figure right side (c), the stress gradients and the hydrostatic pressure gradient are shown; they all were used either as initial or boundary conditions.

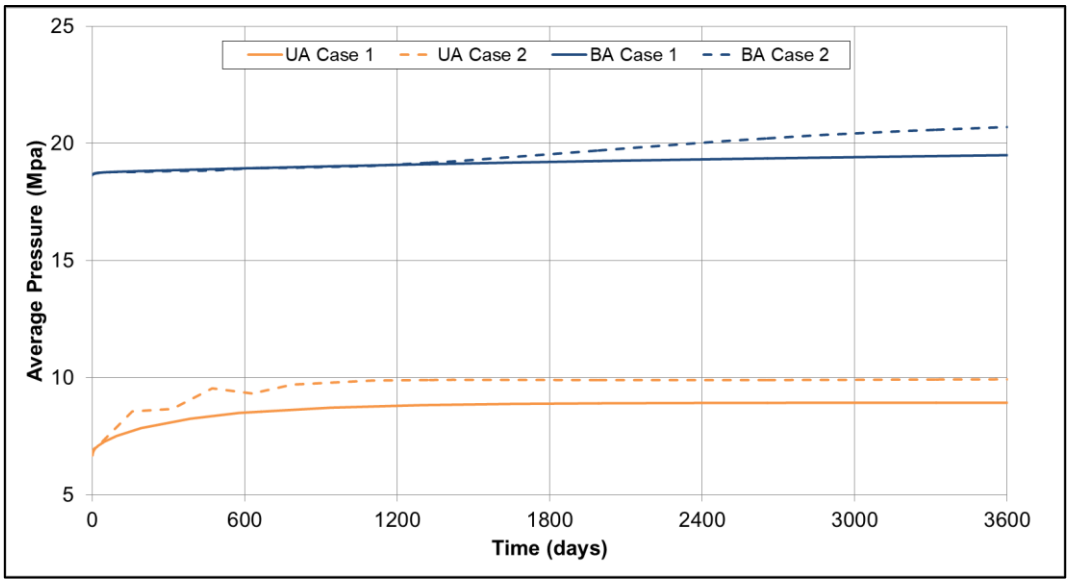

(a) Upper Aquifer (UA) and Basal Aquifer (BA)

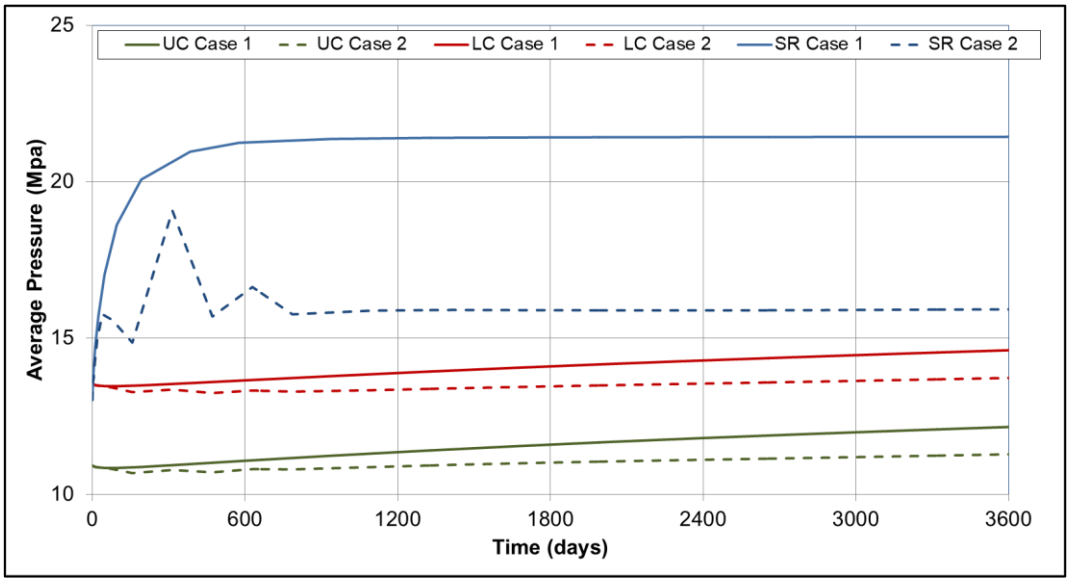

(b) Upper Caprock (UC), Storage Reservoir (SR), Lower Caprock (LC)

Figure 2. The time evolution of average pressure per-layer for two study cases: Case 1 [i.e. without incorporating the evolution of permeability in the faulted zone], and Case 2 [those incorporating the evolution of permeability in the faulted zone (cf. equation 11) resulting in pressure change within all formation units due to flow redistribution]. Acronyms correspond to the geological formation units: Upper Aquifer (UA), Upper Caprock (UC), Storage Reservoir (SR), Lower Caprock (LC), and Basal Aquifer (BA).

5- Conclusions and way forward

This work describes a simple modeling approach to evaluate the risk of fault integrity resulting from fluid injection into deep aquifers. The proposed simulation approach opens a way for a quick numerical estimation of leakage risks through the dynamic analysis of fluid flow in faulted regions. Capturing complex fault behaviors with fast and accurate models could help to support decision-making processes, providing necessary tools for performing reservoir management tasks more efficiently and safely.

The proposed modeling and simulation approach offers the following advantages:

– A fully-integrated modeling approach was successfully developed using the combination of COMSOL Multiphysics interfaces. This approach

provides a framework for performing modeling and simulation studies that consume reasonably short CPU times accounting for problem complexity.

- The model relies on relatively simple modeling choices already implemented in existing commercial and research codes. This allowed initiating the study of complex Multiphysics interactions between reservoir fluid flow and rock mechanics in a reasonable time frame.
- The model incorporates physical mechanisms responsible for the reservoir overpressure, corresponding perturbations of the faulted region state, sufficient mechanical deformations and enhancements of the fault permeability, creating new high-permeability pathways for possible CO_2 leakage.
- It has been demonstrated that a robust fully-coupled simulation approach can successfully be used to solve for the proposed coupled flow and mechanical stress variables. The solution approach is computationally efficient and takes advantage of solver options that improve the convergence of the nonlinear system of equations.

The presented study pointed out that the dynamics of the fault permeability is a critical factor for analyzing potential risks for GCS projects. Our results indicate that dynamic coupled flow and geomechanical modeling is required for the proper estimation of the dynamic permeability enhancement effects due to the volumetric strain evolution.

Finally, further efforts will be necessary to incorporate more accurate constitutive equations considering fault permeability stress and strain dependences. More realistic models should rely on 3D geometries, as for instance 2D geometries tend to affect the horizontal stresses. The model extrapolation to 3D geometries seems (technically) rather straightforward. In addition, the evaluation of multiple scenarios like initially closed, opened or semi-opened fault to fluid flow could also be envisaged. The coupled model is compatible with dynamic probabilistic risk assessment, as it provides physical parameters which may be put into practice using uncertainty quantification methods.

References

1) Rutqvist, J. The Geomechanics of CO_2 Storage in Deep Sedimentary Formations. *Geotech Geol Eng* (2012) Volume 30, Issue 3, Pages 525-551.
2) Bjørnarå, T. I., Aker, E., Cuisiat, F. and E. Skurtveit. Modeling CO_2 storage Using Coupled Reservoir-Geomechanical Analysis, *Proceedings of the COMSOL Conference 2010.* Paris, France (2010).
3) Nguyen, T.S., Guglielmi, Y., Graupner, B., Rutqvist, J. Mathematical modelling of fault reactivation induced by water injection (2019) Minerals, 9 (5), art. no. 282.
4) Fjær, E.; Horsrud, P.; Raaen, A.M.; Risnes, R.; Holt, R.M. (1992). Petroleum Related Rock Mechanics. London: Elsevier Science.
5) Bear, J. (1972). Dynamics of fluids in porous media. New York : American Elsevier.
6) Ihsan G.K. (2018). Study on The Effect of Production Dynamic to Fault Reactivation A Case Study of Groningen Gas Field (Master of Science dissertation). Retrieved from http://repository.tudelft.nl/.
7) Mainguy M. and Longuemare P. (2002). Coupling Fluid Flow and Rock Mechanics: Formulations of the Partial Coupling between Reservoir and Geomechanical Simulators. Oil & Gas Science and Technology – Rev. IFP, Vol. 57, No. 4, pp. 355-367.
8) Cappa, F. and J. Rutqvist. Modeling of coupled deformation and permeability evolution during fault reactivation induced by deep underground injection of CO_2, International Journal of Greenhouse Gas Control, Volume 5, Issue 2, 2011, Pages 336-346, ISSN 1750-5836.
9) Guglielmi, Y. ; Birkholzer, J. ; Rutqvist, J. ; Jeanne, P. and Nussbaum, C. Can Fault Leakage Occur Before or Without Reactivation? Results from an in Situ Fault Reactivation Experiment at Mont Terri, *Energy Procedia*, Volume 114, 2017, Pages 3167-3174, ISSN 1876-6102.
10) Ghanimi, M.A., Leroy, Y.M., Kamp, A.M. Stress-Sensitive Permeability: Application to Fault Integrity During Gas Production (2017) *Transport in Porous Media*, 118 (3), pp. 345-371.
11) COMSOL Multiphysics, Subsurface Flow Module User's Guide. Version: COMSOL 5.4 (2018).

Acknowledgements

The author thanks Yves M. Leroy of TOTAL S.A. for useful discussions of this topic and insightful comments on the paper. TOTAL S.A. is gratefully acknowledged for sponsoring our research work.

Case 1: <u>Without</u> permeability enhancement in the Faulted region

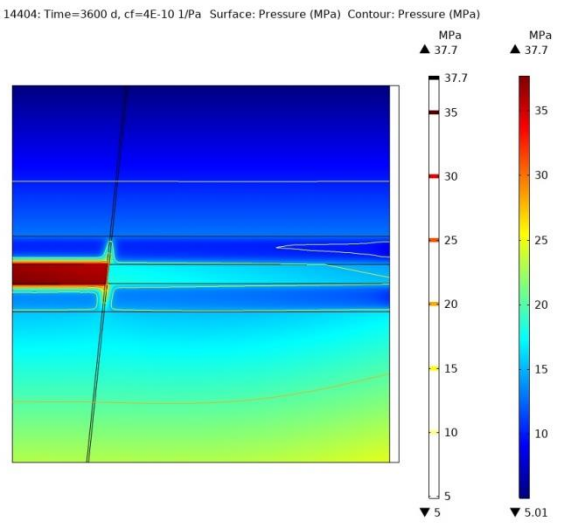

(a) Case 1: Pressure Field

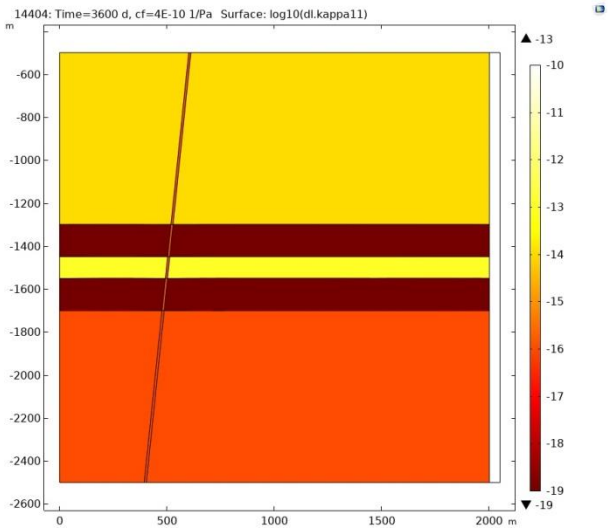

(b) Case 1: Permeability Field

Case 2: <u>With</u> permeability enhancement in the Faulted region

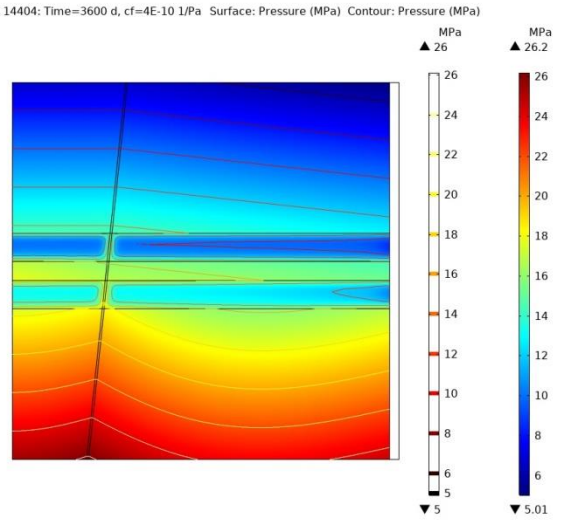

(c) Case 2: Pressure Field

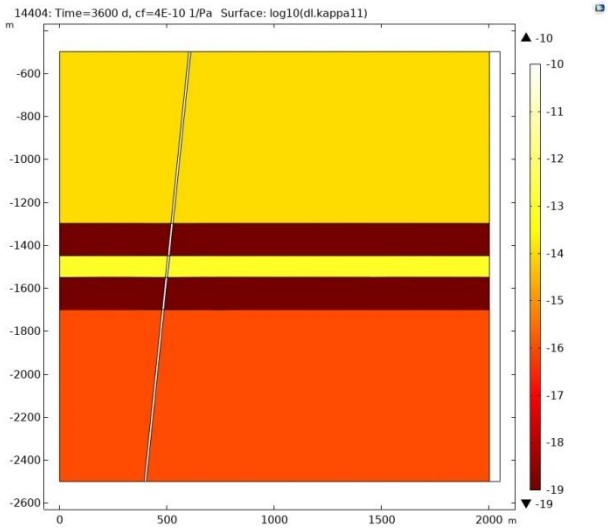

(d) Case 2: Permeability Field

Figure 3. 2D filled-map and contours in terms of the pressure fields (left column) and filled-contours of the permeability fields -in logarithmic scale- (right column). Result snapshots are after 10 years of injection. In the top row, Figures 3a and 3b show the results for Case 1 (without permeability enhancement in the Faulted region). In the bottom row, Figures 3c and 3b show the results for Case 2 (with permeability enhancement in the Faulted region). Permeability is shown in logarithmic scale.

Table 1: List of model parameters

Fluid and well parameters	**Value**
Mass flowrate	0.02 kg/(m·s)
Fluid density	999.55 kg/m³
Fluid Viscosity	0.001 Pa·s
Fluid compressibility	$4.0*10^{-10}$ 1/Pa
Faulted-zone parameters	**Value**
Fault Porosity	0.1
Fault Permeability	10^{-16} m²
Friction angle	25 deg
Dilation angle	20 deg
Cohesion	0
Fault inclination	80 deg
Upper Aquifer parameters	**Value**
Porosity	0.10
Permeability	10^{-14} m²
Top	-500m
Caprock parameters	**Value**
Porosity	0.01
Permeability	10^{-19} m²
Top- Upper Caprock	-1300m
Top- Lower Caprock	-1550m
Storage Aquifer parameters	**Value**
Porosity	0.10
Permeability	10^{-13} m²
Top	-1450m
Base Aquifer parameters	**Value**
Porosity	0.02
Permeability	10^{-16} m²
Top	-1700m